Received: 20 August 2023 | Revised: 16 November 2023 | Accepted: 21 November 2023
DOI: 10.1111/jfd.13900

RESEARCH ARTICLE

Journal of Fish Diseases WILEY

# Magnetic resonance imaging shows spinal curvature in Chinook salmon (*Oncorhynchus tshawytscha*) is associated with chronic inflammation of peri-vertebral soft tissues

Bailey A. Lovett[1,2] | Elwyn C. Firth[1] | Matthew R. Perrott[3] | John S. Munday[3] | Beau P. Pontre[1] | Anna-Maria P. Lydon[1] | Jane E. Symonds[2] | Mark A. Preece[4] | Neill A. Herbert[1]

[1]University of Auckland, Auckland, New Zealand
[2]Cawthron Institute, Nelson, New Zealand
[3]Massey University, Palmerston North, New Zealand
[4]The New Zealand King Salmon Company Limited, Nelson, New Zealand

**Correspondence**
Bailey A. Lovett, Cawthron Institute, 98 Halifax Street East, Nelson 7010, New Zealand.
Email: bailey.lovett@cawthron.org.nz

**Funding information**
Callaghan Innovation, Grant/Award Number: NZKSC1401; University of Auckland, Institute of Marine Science, Grant/Award Number: 35023.001; Ministry for Primary Industries Sustainable Farming Fund (SFF), Grant/Award Number: #13/003

## Abstract

Chinook salmon (*Oncorhynchus tshawytscha*) farmed in New Zealand are known to develop abnormal spinal curvature late in seawater production. Its cause is presently unknown, but there is evidence to suggest a neuromuscular pathology. Using magnetic resonance imaging (MRI), we evaluated the relationship between soft tissue pathology and spinal curvature in farmed Chinook salmon. Regions of interest (ROIs) presenting as pathologic MRI signal hyper-intensity were identified from scans of 24 harvest-sized individuals: 13 with radiographically-detectable spinal curvature and 11 without. ROIs were excised from individuals using anatomical landmarks as reference points and histologically analysed. Pathologic MRI signal was observed more frequently in individuals with radiographic curvature (92%, $n=12$) than those without (18%, $n=2$), was localized to the peri-vertebral connective tissues and musculature, and presented as three forms: inflammation, fibrosis, or both. These pathologies are consistent with a chronic inflammatory process, such as that observed during recovery from a soft tissue injury, and suggest spinal curvature in farmed Chinook salmon may be associated with damage to and/or compromised integrity of the peri-vertebral soft tissues. Future research to ascertain the contributing factors is required.

KEYWORDS
Chinook salmon, chronic inflammation, finfish skeletal health, MRI, neuromuscular pathology, spinal curvature

## 1 | INTRODUCTION

The prevention and minimisation of spinal deformities in farmed finfish constitutes an important management priority for the aquaculture industry (Boglione et al., 2013; Divanach et al., 1996; Fjelldal et al., 2007; Fjelldal, Hansen, et al., 2009; Fjelldal, van der Meeren, et al., 2009; Koumoundouros, 2010; Sullivan et al., 2007; Vagsholm & Djupvik, 1998; Waagbø et al., 2005; Witten et al., 2009). Affected individuals often cannot be marketed at a premium price and frequently require additional processing (Sullivan et al., 2007; Vagsholm

& Djupvik, 1998). In severe cases, swimming and feeding abilities may be compromised, leading to impaired growth, reduced harvest weights, and welfare concerns (Branson & Turnbull, 2008; Hansen et al., 2010; Huntingford et al., 2006; Silverstone & Hammell, 2002). However, the aetiology of spinal deformities is complex and typically multifactorial, with the individual effects of contributing factors difficult to disentangle in commercial farming environments (Vagsholm & Djupvik, 1998; Waagbø et al., 2005; Witten et al., 2009). Determining the cause(s) of spinal deformities in farmed finfish, and subsequently reducing their prevalence, can therefore be highly challenging. However, knowledge of their pathology can help to identify causative factors.

Spinal deformities can be broadly divided into two groups – those which primarily affect the structure of individual vertebral bodies, such as fusions, compressions, vertical shifts, and fractures, and those which alter the entire spinal axis, such as spinal curvatures (lordosis, kyphosis, and scoliosis) (Fjelldal et al., 2007). While the former are considered to predominantly arise via skeletogenic (bone development-related) mechanisms, the latter are proposed to have a neuromuscular origin, especially where the structure of the involved vertebral bodies is unchanged (Witten et al., 2009). Despite this, the established diagnostic tools for characterizing spinal pathology in fish (i.e., X-ray) mainly assess only bone, and those currently used to evaluate soft tissues (e.g., histology, immunohistochemistry) are highly invasive. Sampling therefore often requires euthanasia, preventing the observation of tissue changes over time. This inevitably presents difficulties when attempting to characterize the development of deformities with a suspected neuromuscular pathology. However, there appears to be little research dedicated to exploring alternative tools that can detect and evaluate such pathologic soft tissue changes in finfish.

In humans and other mammals, such as horses (Dyson et al., 2005; Mitchell et al., 2012; Tucker & Sande, 2001; Zubrod et al., 2004), monkeys (Wei et al., 2014), dogs (da Costa, 2010; Gnirs et al., 2003; Grünenfelder et al., 2005), cats (Asperio et al., 1999; Gonçalves et al., 2009; Lu et al., 2002; MacKay et al., 2005) and rabbits (Keeble, 2006), computed tomography (CT) and magnetic resonance imaging have become increasingly used in the clinical diagnosis and characterization of musculoskeletal conditions. Compared to X-ray, MRI and CT are vastly more sensitive in their detection of pathologic tissue changes, with CT preferred for evaluation of bony structures and MRI for soft tissues including the spinal cord, peri-vertebral muscle, connective tissues, nerves, tendons, and ligaments (Mahoney, 2012; Theodorou et al., 2012). MRI in particular has fast become regarded as the "gold standard" of imaging modalities in the diagnosis of muscle trauma, atrophy, and disease (Garcia, 2000). This is largely owing to its superior differentiation of muscular tissues compared to CT and other imaging modalities, as well as its multi-planar display and lack of ionizing radiation (Garcia, 2000; Joseph & Habib, 2009; Kattapuram et al., 2005; Steinbach et al., 1994). Consequently, MRI is frequently used to detect, diagnose, and monitor the progression of a wide variety of musculoskeletal diseases, guide biopsy in regions of active disease, and evaluate the effectiveness of applied treatments over time at a greatly reduced cost and level of patient discomfort compared to the more traditional repeated biopsy approach (Garcia, 2000; Murphy et al., 1986; Theodorou et al., 2012; Winkler et al., 2011).

In New Zealand, farmed adult Chinook (king) salmon (*Oncorhynchus tshawytscha*) are known to develop spinal curvatures late in the seawater production cycle in the form of lordosis (ventrad curvature), kyphosis (dorsad curvature) and scoliosis (lateral curvature). While individuals can develop each of the curvature types in isolation, harvest-size individuals frequently present with all three types. This condition, known as LKS (lordosis-kyphosis-scoliosis), poses both economic and welfare concerns (Lovett et al., 2020; Perrott et al., 2018)—affected individuals have reduced swimming performance, compromised growth and, due to their visual appearance, cannot be marketed at a premium (Lovett et al., 2020; Perrott et al., 2018). While various factors have been proposed to contribute to spinal curvature development in farmed New Zealand Chinook salmon, including mechanical imbalance and/or overload from excessive musculature , fast growth, elevated water temperature, and high weight-to-length ratio (i.e., condition factor) (Lovett et al., 2019; Munday et al., 2016; Perrott et al., 2018; Scholtens et al., 2023), the primary cause remains unknown. However, the condition has been found to be associated with the presence of localised unilateral peri-vertebral muscle fibrosis and inflammation (Munday et al., 2016) and reduced integrity of the peri-vertebral muscle connective tissues (Perrott et al., 2020). Using histology, Munday et al. (2016) observed that peri-vertebral fibrosis was more frequently detected in individuals with visually detectable spinal curvature than those without, and radiographic spinal curvature and fibrosis severity scores were strongly positively correlated. It was therefore proposed that inflammation of unknown causes drives the development of unilateral peri-vertebral muscle fibrosis, which subsequently results in curvature of the spine. In a more recent study, Perrott et al. (2020) found that the peri-vertebral muscle of New Zealand Chinook salmon from a farmed population with a high incidence of curvature had a significantly lower Type I collagen content and a less mature collagen cross-link profile (both indicative of reduced connective tissue integrity) than individuals from a farm with a low curvature incidence. These observations have led to the hypothesis that the primary pathology of the condition is neuromuscular. However, as standardized locations for sampling were used in both studies, which were not necessarily related to the location of curvature, a direct link between these observed pathologic soft-tissue changes and curvature has not yet been established. There is therefore a need to further explore the nature of the association between pathologic soft-tissue changes and spinal curvature development in this species.

Although MRI has been conducted on finfish previously (e.g., Bock, Sartoris & Pörtner, 2002; Bock, Sartoris, Wittig, et al., 2002; Collewet et al., 2013; Howell et al., 1996; Lannig et al., 2004; Mark et al., 2002; Pörtner et al., 2004; Rogers et al., 2008; Simões et al., 2012; Van der Linden et al., 2004; Wu et al., 2015), including for the purposes of diagnosing musculoskeletal pathology (Torpy et al., 2023), it has not yet been applied to the diagnosis of musculoskeletal pathology in commercially farmed finfish. The aim of the current study was to use MRI to assess peri-vertebral soft-tissue pathology in farmed New Zealand Chinook salmon and, in conjunction with histology, evaluate its association with spinal curvature. It was hypothesised that areas of MRI signal hyper-intensity would be associated with spinal curvature and, in accordance with previous findings (Munday et al., 2016), would correspond to inflammation and fibrosis on histology.

## 2 | MATERIALS AND METHODS

### 2.1 | Rearing and selection of fish

This work was carried out in accordance with the Animal Welfare Act 1999 and on-farm industry animal welfare regulations. Whole-body carcasses of 24 commercially farmed adult (2–2.5 years old) female Chinook salmon (1800–4440 g body weight [BW]) were collected between May and September 2016 from harvest operations of two sea pens located at Ruakaka Bay (41°11′38.121″ S 174°6′51.74″ E) ($n=18$) and Te Pangu Bay (41°15′19.369″ S 174°14′20.661″ E) ($n=6$) in the Marlborough Sounds, New Zealand. Fish in both pens had been reared under a standard production regime and fed to satiation on the same commercial pellet-based diet averaging (per 100 g feed): 44.2% protein, 24.0% fat, 16.9% carbohydrate; 31.9% fishmeal, 7.1% fish oil; 1.24 mg $kg^{-1}$ phosphorus (P), and 1000 mg vitamin C. Fish had been fed 10 meals per day for the first month in seawater, five per day up to 250 g average body weight (BW), three per day from 250 g to 1 kg BW and two per day from 1 kg BW to harvest. As per Lovett et al. (2019), individuals were identified as either affected or unaffected by spinal curvature based on visual examination and palpation, and selected accordingly. Affected individuals ($n=12$) were selected first, weighed (Tru-Test™ XR-5000 digital scales), measured (fork length, FL) and laterally radiographed (60 kV and 0.10 mAs, Atomscope HF80/15 + DLP and Sound® Canon® Tru-DR™ receiver plate set at 50 cm distance). The same procedure was then carried out on selected unaffected individuals ($n=12$), each of which was matched by body weight with an affected individual due to the difficulties in accurately measuring the length of affected individuals.

### 2.2 | Radiological assessment of spinal curvature

Prior to MRI scanning, radiographs of each individual were assessed to confirm the presence/absence of spinal curvature. All 12 visually affected individuals, as well as one visually unaffected individual, had radiographic spinal curvatures (rSC). The final study population ($n=24$) therefore consisted of 13 (radiographically) affected (mean BW = 3132 ± 199 g) and 11 unaffected fish (mean BW = 2797 ± 216 g). *T*-tests showed there were no statistically significant differences in weight ($p=.49$) or Fulton's condition factor (calculated as $100 \times BW/FL^3$) between affected and unaffected individuals ($p=.49$ and .11, respectively). Radiographic curvature was scored according to existing protocols (Lovett et al., 2020; Munday et al., 2016; Perrott et al., 2018; Witten et al., 2009). The number of curvatures was recorded for each affected individual, as well as the spinal region (region (R)1 = vertebra (V)1–8, R2 = V9-31, R3 = V32-50, R4 = V51-62+) affected and type(s) of curvature (lordosis, kyphosis, and/or scoliosis) present. Variation in total vertebral number between individuals was captured in R4. Where a given curvature spanned multiple spinal regions, the region in which the apex of the curvature was located was assigned as the region for that curvature. The presence of other non-curvature spinal anomalies commonly observed in Chinook salmon (i.e., vertebral compressions, fusions, and vertical shifts) was also noted but not investigated further, as the current research concerned only curvature.

### 2.3 | MRI scan image acquisition

MRI scanning was carried out approximately 12 h after death. Two small incisions ~2 cm deep were made in the dorsal surface of each individual immediately prior to MRI scanning; one 2 cm to the left of the anterior origin of dorsal fin and the other 2 cm to the left of the adipose fin. A fish-oil capsule (Healtheries® Fish Oil 1500 mg) was then inserted into each cavity to provide an internal MRI-detectable reference point. Each individual was placed head-first, left side-down on the bed of a 3T MAGNETOM Skrya MRI scanner (Siemens Healthineers) equipped with an in-built spine matrix coil, and covered with an 18-channel body matrix coil (Body 18). MRI scan images were acquired using a T2-weighted isotropic 3D turbo spin echo SPACE (Sampling Perfection with Application Optimized Contrasts using different flip angle Evolution) scan sequence (Table 1). Planar image reconstructions were obtained from the acquired image data in both the sagittal plane ($n=88$–96 images per individual) and axial plane ($n=316$–386 images per individual). Following scanning, fish were placed back on ice and chilled overnight at 4°C.

### 2.4 | MRI scan image assessment and ROI determination

Sagittal and transverse MRI scans of each individual were evaluated with *syngo* fastView (Siemens AG Medical Solutions) and Horos (The Horos Project, www.horosproject.org) using the axial plane scans as localisers. Contrast was optimized for each individual series of images by manually adjusting window width (WW) and window length (WL) prior to assessment. Scans of individuals affected and unaffected by radiographic curvature were examined and scored for the presence/absence of pathologic MRI signal intensity, which was defined as signal hyper-intensity not associated with typical Chinook salmon anatomy (e.g., intervertebral discs, intramuscular adipose

**TABLE 1** Parameters for T2-weighted isotropic 3D turbo spin echo SPACE (Sampling Perfection with Application Optimized Contrasts using different flip angle Evolution) magnetic resonance imaging (MRI) of Chinook salmon (*Oncorhynchus tshawytscha*) unaffected (U, $n = 11$) and affected (A, $n = 13$) by radiographic spinal curvature.

| MR pulse sequence | # of fish scanned | Matrix | FOV (mm) | TI (ms) | TR (ms) | TE (ms) | Flip angle (°) | ETL | Resolution (mm) | Slice thickness (mm) | NEX |
|---|---|---|---|---|---|---|---|---|---|---|---|
| SPACE | 24 (13 A, 11 U) | 512×205 | 390×105 | – | 1700 | 85 | 160 | 56 | 0.8×0.8×0.6 | 0.60 (sagittal)<br>1–3[a] (axial)<br>1 (axial) | 2 |

*Note*: $n = 24$.

Abbreviations: ETL, echo train length; FA, flip angle; FOV, field of view; NEX, number of averages; TE, echo time; TI, inversion time; TR, repetition time.

[a]Slice thickness for axial images of one group of individuals was 3 mm, not 1 mm.

tissue, see Figure 1). Where detected, the nature of the pathologic signal, as well as its location relative to both established spinal regions (R1, R2, R3, R4) and anatomical landmarks (i.e., fins, gut, etc.), and its association with radiographic spinal curvature (yes/no and if yes, the location and type of associated curvature), were also recorded.

## 2.5 | Carcass dissection

Identified regions of pathologic MRI signal hyper-intensity, henceforth referred to as regions of interest (ROIs), were dissected out of individuals ~12 h post-MRI. Tissue blocks associated with identified ROIs were dissected from radiographically affected individuals first, using anatomical landmarks and MRI scan images as a guide. Where no hyper-intense MRI signal was detected in a particular spinal region (i.e., R1, R2, R3, R4), a standardized ~3 vertebrae long sample block corresponding to the mid-point of the unaffected location was excised, as per Munday et al. (2016). Sample blocks corresponding to the location of ROIs in each affected individual were then dissected out of the corresponding (i.e., weight-matched) radiographically unaffected individual, as well as any ROIs observed in the unaffected individuals. Excised blocks were weighed (g), then fully immersed in 400–700 mL (depending on tissue block size) of 10% neutral-buffered formalin (ThermoFisher Scientific Ltd).

## 2.6 | Tissue decalcification and histological analysis

Extracted samples were decalcified and paraffin-embedded according to standard protocols. Due to their size, each block was subdivided into 2–4 samples of approximately equal size. Samples were then cut into 4 µm sections and stained with haematoxylin and eosin (Leica® Autostainer XL). Mounted sections were examined with a compound microscope by an experienced pathologist familiar with histological changes associated with spinal curvature pathology in Chinook salmon, and any pathologic changes (i.e., deviation from presentation of histologically normal tissue) were described and recorded. These broadly comprised presence or absence of basophilic material and fluid (indicative of inflammation), blood vessel proliferation, changes to the structural appearance of intervertebral ligaments, vertebral bone and peri-vertebral muscle, and the structure of collagen fibres present (i.e., mature/immature).

## 2.7 | Data and statistical analysis

Results were reported as means ± standard error (SE) for continuous data, and as median values for discrete data. Statistical significance was accepted at $p < .05$. Fisher's exact tests with post-hoc Bonferroni correction were used to evaluate associations of MRI ROI type with spinal curvature type and histopathology type, respectively.

Journal of Fish Diseases 

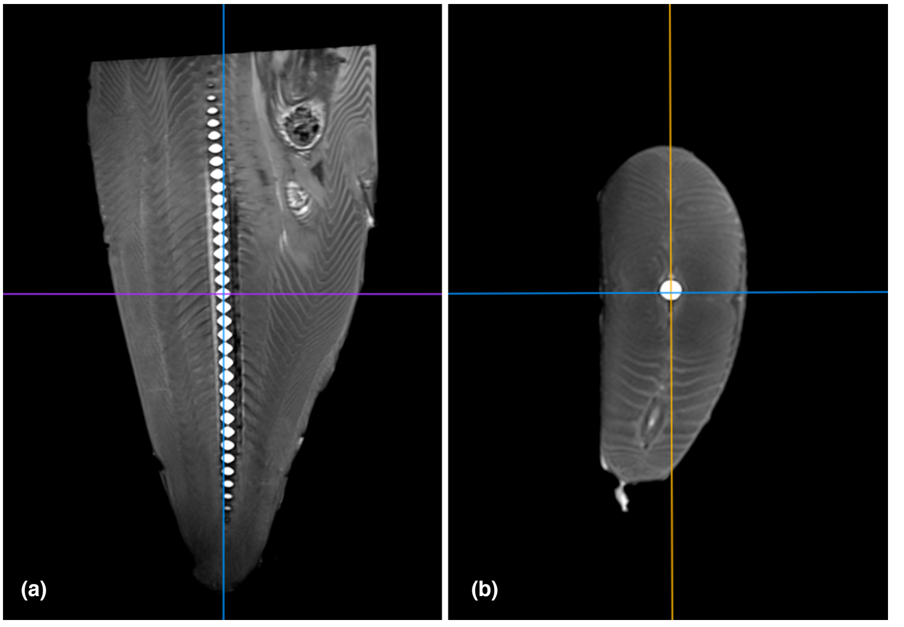


**FIGURE 1** Non-pathologic magnetic resonance signal in Chinook salmon. Sagittal (a) and axial (b) T2-weighted SPACE magnetic resonance images of an adult Chinook salmon *Oncorhynchus tshawytscha* (body weight = 3150 g, fork length = 57 cm) showing non-pathologic signal hyper-intensity associated with the intervertebral discs (crosshairs). Location of crosshairs in a corresponds to that of crosshairs in b.

# 3 | RESULTS

## 3.1 | Radiological (X-ray) observations

Fifty-five curvatures were observed across the 13 individuals with rSC (Table 2). The number of curvatures per individual ranged from 1 to 9. Curvatures were found in all spinal regions, but primarily manifested in R2 and R3. Lordosis and kyphosis occurred with a similar frequency, with lordosis mainly observed in R1 and R3 and kyphosis in R2 and R4. Scoliosis was less prevalent than the other two types, and predominantly occurred in R3.

## 3.2 | MRI scan observations

Sixty ROIs corresponding to MRI signal hyper-intensity were detected on T2-weighted MRI scans of 12 individuals with rSC and two without rSC (Table 3). The number of ROIs per individual ranged from 1 to 7, but was higher for individuals with rSC. Most ROIs were observed in the posterior spinal regions, predominantly R3.

Of the body regions without pathologic MRI signal hyper-intensity that were also sampled ($n$ = 88), most (73%, $n$ = 64) were from individuals without rSC.

Three discernible types of MRI signal hyper-intensity were observed within the identified ROIs. Type A (Figure 2) presented as a distinct unilateral hyper-intensity which was highly localized to the periphery of the spinal column, though it frequently proliferated out along the horizontal, and occasionally vertical, septum. In contrast, Type B (Figure 3) presented as dull "cloudy" signal that was not localized to the spinal column or unilateral. Although this signal type rarely affected either septum, on axial scans, it was often observed to infiltrate the peri-vertebral muscle blocks. Both signal types were clearly visible on axial scans. Type B was less detectable on sagittal scans than Type A, but often presented in this plane as scattered black and grey patches. Large Type A lesions, especially those which proliferated out into the horizontal septum, presented as thick bright lines on sagittal scans, while small lesions confined to the peri-vertebral area presented as small bright white dots in this plane.

ROIs detected in some individuals possessed elements of both Types A and B and were thus designated as a third signal type, C (Figure 4). As in Type A, Type C signal presented as bright hyper-intensity which expanded into the horizontal septum, but was also accompanied by a duller, less distinct Type B-like hyper-intensity that extended from the peri-vertebral connective tissues into the surrounding muscle.

Of the 60 ROIs identified on MRI scans, 43 (72%) were Type A, 13 (22%) were Type B and 4 (7%) were Type C. Most individuals with detectable MRI ROIs possessed only Type A (71%, $n$ = 9), with one individual having Type B only, 2 having both A and B, and 2 having all three types. Irrespective of type, MRI hyper-intensity was more frequently observed where curvatures were present than not, with 43 of the 60 ROIs (72%) located in spinal regions where at least one curvature was detected. The remaining 17 ROIs that occurred in regions without curvatures were from two individuals without rSC ($n$ = 4, all Type A) and a further four individuals with mild rSC.

There was no significant association between MRI ROI type and the type of curvatures found in the region the ROI was detected in $p$ = .99. However, Type A lesions observed in scoliotic regions appeared to occur exclusively on the concave side of the scoliotic curve. No such observations were apparent for regions of lordosis or kyphosis.

## 3.3 | Histopathology

Histological lesions were visible in 46 (77%) of the 60 samples taken from MRI ROIs. In contrast, histological lesions were only observed in 4 (5%) of the 88 samples taken from regions without pathologic MRI signal hyper-intensity. Two of these samples were from one individual without rSC and the other two from the individual that had radiographic, but not visual, rSC.

TABLE 2 Occurrence of radiographic spinal curvature (rSC) types (L = lordosis, K = kyphosis, S = scoliosis) in spinal regions R1–R4 (R1 = vertebra (V)1–8, R2 = V9-31, R3 = V32-50, R4 = V51-62+) of farmed adult Chinook salmon (*Oncorhynchus tshawytscha*).

| | Spinal region | | | | |
|---|---|---|---|---|---|
| Spinal curvature type | R1 | R2 | R3 | R4 | Total |
| L | 6 | 3 | 9 | 3 | 21 |
| K | 0 | 9 | 1 | 10 | 20 |
| S | 2 | 4 | 7 | 1 | 14 |
| Total | 8 | 16 | 17 | 14 | 55 |

*Note*: $n = 13$.

Three distinct types of histological lesions were observed. The first was classified as Type 1 (Figure 5) and appeared as expansion of the peri-vertebral connective tissues, especially the horizontal septum, with large quantities of loosely-arranged connective tissue, which sometimes presented within a background of basophilic material. The arrangement of the connective tissue and the basophilic appearance of the surrounding tissue was consistent with early fibrosis within an area of high fluid content. As this reaction was often confined to the peri-vertebral connective tissue that extended into the horizontal septum, it often appeared as a 'Y'-shaped pale area within the sections. The early fibrosis and basophilic material was confined to the connective tissues and rarely extended into the surrounding skeletal muscle.

Type 2 histological lesions were defined by the presence of connective tissue infiltrating the peri-vertebral skeletal muscle (Figure 6). In contrast to the connective tissue within Type 1 lesions, the infiltrating connective tissue was more densely and regularly arranged and was not associated with basophilic background material.

TABLE 3 Regions of signal hyper-intensity (ROIs) detected on sagittal and axial T2-weighted SPACE magnetic resonance scan images of farmed adult Chinook salmon (*Oncorhynchus tshawytscha*) with and without radiographic spinal curvature (rSC).

| | | | | | ROI spinal region | | | |
|---|---|---|---|---|---|---|---|---|
| Group | *N* | # individuals with ROIs | Total # ROIs | Median # ROIs per individual | R1 | R2 | R3 | R4 |
| No rSC | 11 | 2 | 4 | 2 | 0 | 0 | 2 | 2 |
| rSC | 13 | 12 | 56 | 5 | 2 | 13 | 27 | 14 |
| All | 24 | 14 | 60 | 4.5 | 2 | 13 | 29 | 16 |

*Note*: $N = 24$.

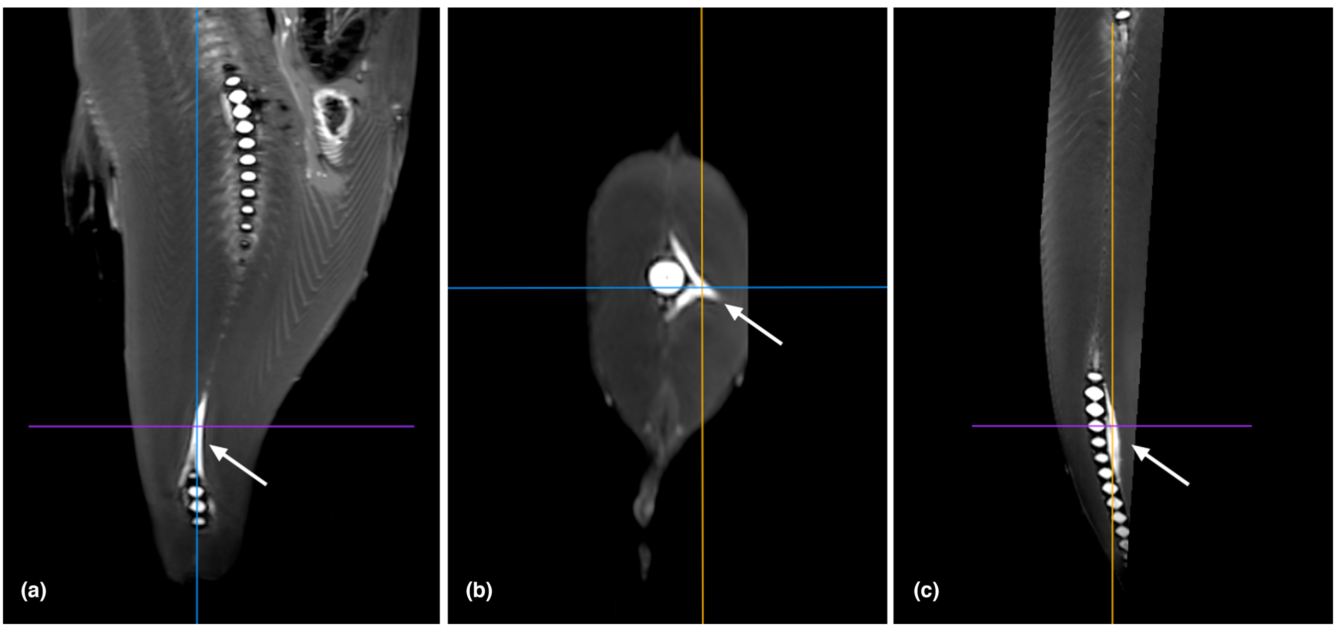


FIGURE 2 Type A pathologic magnetic resonance signal in Chinook salmon. Type A signal hyper-intensity (white arrows) as observed on sagittal (a), axial (b) and coronal (c) T2-weighted SPACE magnetic resonance scans of a farmed adult Chinook salmon (*Oncorhynchus tshawytscha*) (body weight = 3810 g, fork length = 57 cm). Type A presented as a distinct hyper-intense signal which was unilateral and highly localized to the peri-vertebral region, particularly the horizontal septum. Location of crosshairs in a corresponds to that of crosshairs in b and c.

Journal of Fish Diseases -WILEY

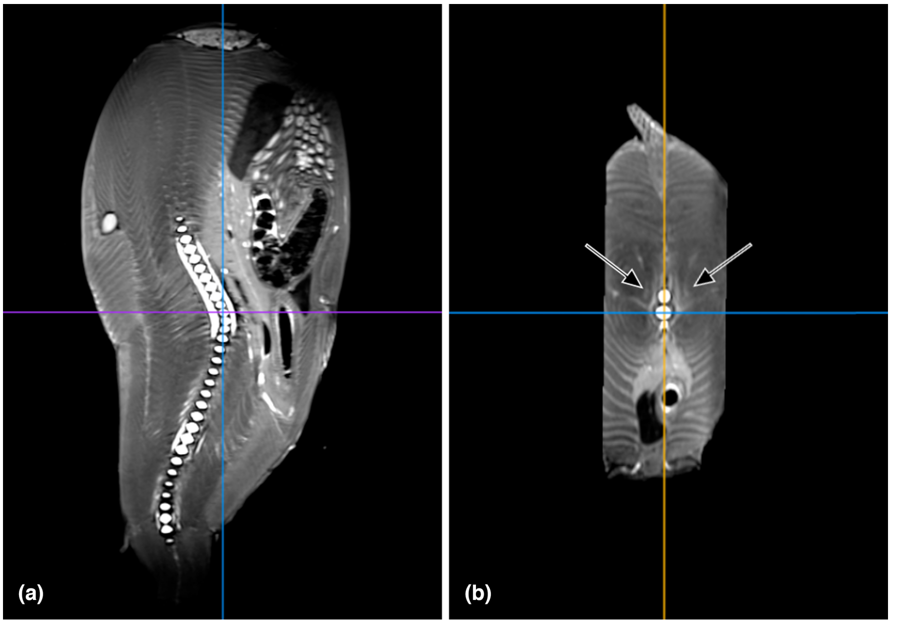


**FIGURE 3** Type B pathologic magnetic resonance signal in Chinook salmon. Type B signal hyper-intensity (black arrows with white outline) as observed on sagittal (a) and axial (b) T2-weighted SPACE magnetic resonance scans of a farmed adult Chinook salmon (*Oncorhynchus tshawytscha*) (body weight = 2760 g, fork length = 52 cm). Type B presented as dull "cloudy" signal which was not localized to the peri-vertebral region and often proliferated into the surrounding skeletal musculature. Location of crosshairs in a corresponds to that of crosshairs in b.

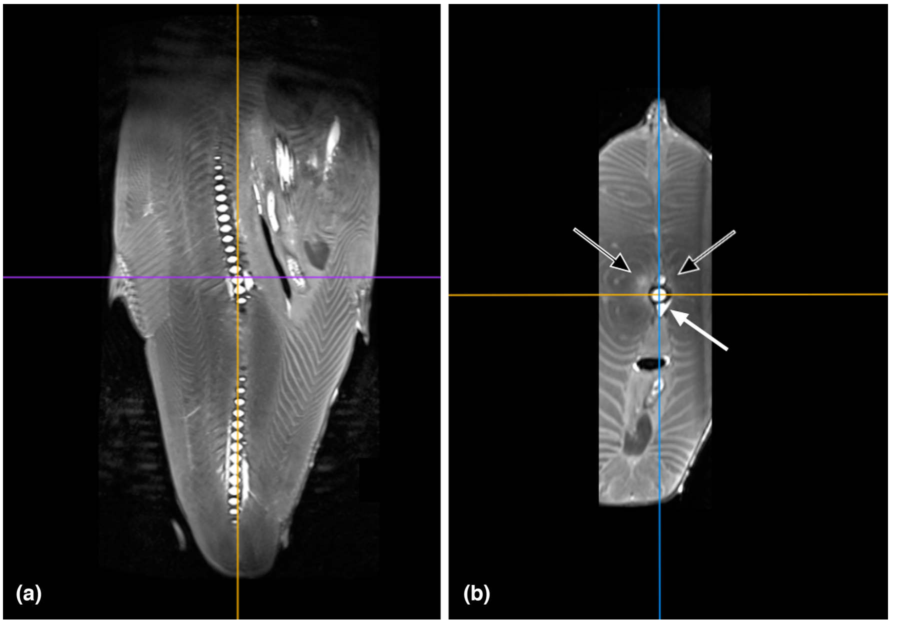


**FIGURE 4** Type C pathologic magnetic resonance signal in Chinook salmon. Type C signal hyper-intensity as observed on sagittal (a) and axial (b) T2-weighted SPACE magnetic resonance scans of farmed adult Chinook salmon (*Oncorhynchus tshawytscha*) (body weight = 4440 g, fork length = 57 cm). Type C hyper-intensity presented as a combination of both Type A (b, white arrow) and Type B (b, black arrows with white outline) signal hyper-intensity. Location of crosshairs in a corresponds to that of crosshairs in b.

The dense connective tissue was sometimes attached to the periosteum of the vertebra, but this feature was not present in all sections. The connective tissue infiltrated between muscle fibres, with separation of fibres often visible. A significant proportion of the peri-vertebral muscle was replaced by fibrosis in some sections.

Some sections had features of both Type 1 and Type 2 lesions. For many of these sections, either the degree of intramuscular fibrosis or the degree of expansion of the connective tissue by loose fibrous tissue was more prominent and these were classified using the predominant feature. However, some had significant changes that represented both Type 1 and 2 classifications, and these were classified separately as Type 3.

Of the three histological types, Type 1 lesions were observed most frequently, with 25 (54%) of the 46 samples taken from MRI ROIs having histological lesions of this type (Table 4). Fifteen (33%) of the 46 MRI ROIs with histological lesions had Type 2, and the remaining 6 (13%) had Type 3. All 4 (100%) of the samples taken from regions without pathologic MRI signal that had histological lesions had Type 1. Of the 14 MRI ROIs that did not have histological lesions, 10 (71%) were Type A and 4 (29%) were Type B.

There was a significant association between MRI ROI type and histological lesion type (Fisher's exact test, $p < .001$). Post-hoc comparisons using Bonferroni correction revealed that Type A ROIs were significantly associated with Type 1 lesions ($p = .05$), and Type B ROIs with Type 2 lesions ($p = .01$). While Type C ROIs were most frequently associated with Type 3 histological lesions, the association was not significant ($p = .47$).

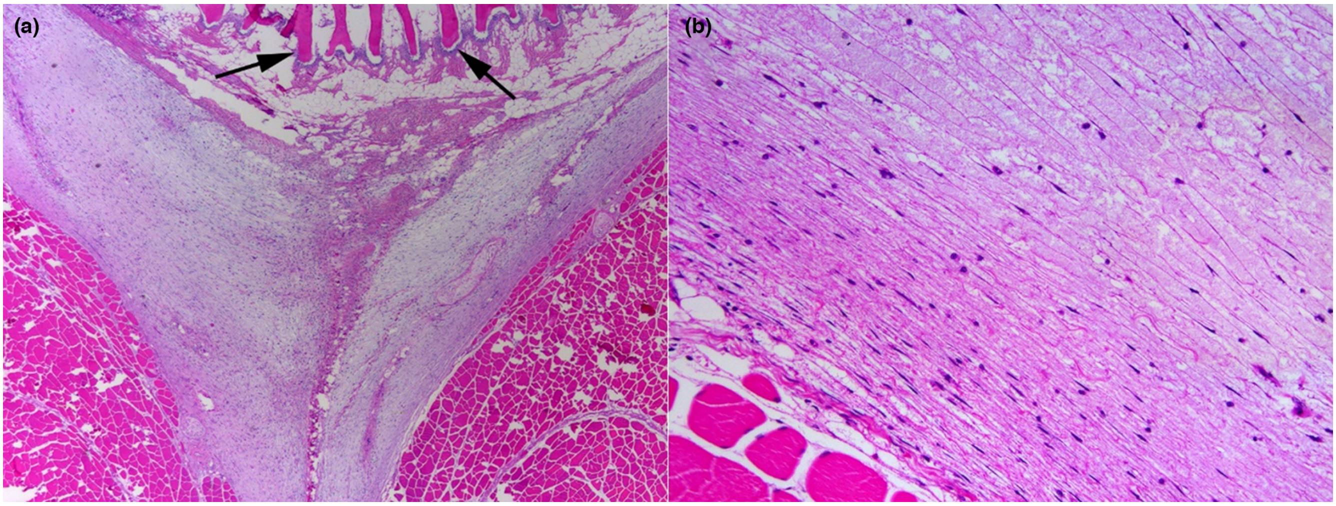


FIGURE 5 Type 1 histological changes associated with pathologic magnetic resonance signal in Chinook salmon. (a) The horizontal septum and peri-vertebral connective tissues are expanded by loosely arranged connective tissue and pale basophilic material. The brightness of this material within the MR scans is consistent with a high water content within these areas. The expansion results in a 'Y'-shaped dilation of the connective tissue immediately adjacent to the vertebral bone (arrows), which could also be observed on the corresponding MRI scan. H & E 25× magnification. (b) The horizontal septum is expanded by loose connective tissue. Note that the reaction is confined to the peri-vertebral connective tissue and does not significantly involve the adjacent skeletal muscle (lower left corner of the photomicrograph). H & E 200× magnification.

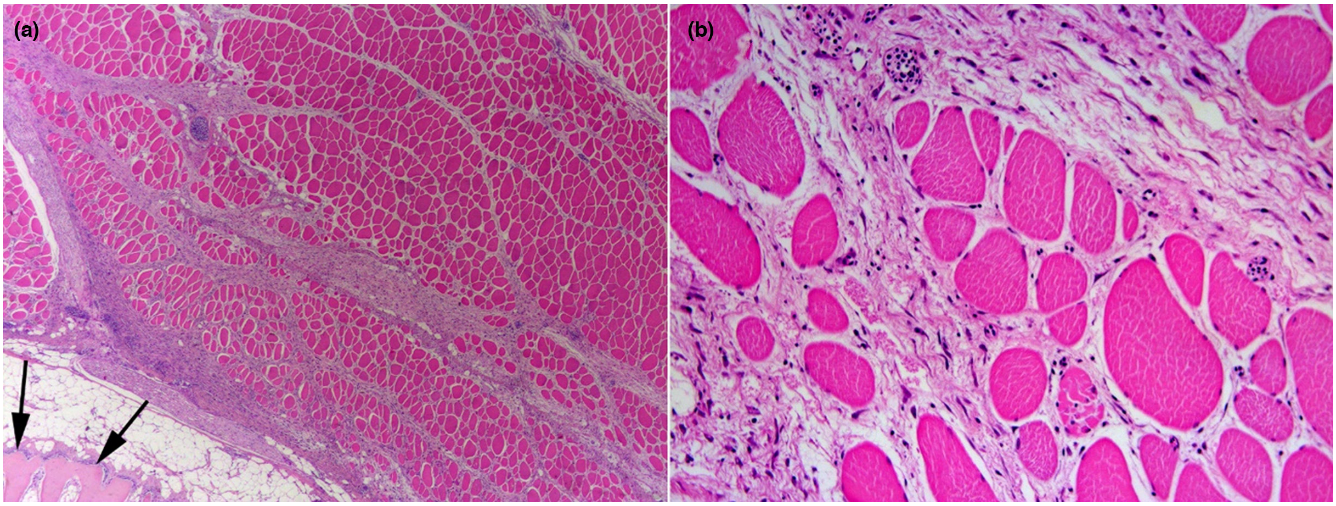


FIGURE 6 Type 2 histological lesions associated with pathologic magnetic resonance signal in Chinook salmon. (a) The peri-vertebral connective tissue contains increased quantities of dense connective tissue that extends into the surrounding skeletal muscle. The horizontal septum is not significantly expanded. Vertebral bone is indicated by arrows. H & E 25× magnification. (b) The dense connective tissue surrounds muscle bundles, but also infiltrates within muscle bundles causing separation of individual muscle fibres. H & E 200× magnification.

## 4 | DISCUSSION

The results show that MRI was able to detect peri-vertebral soft-tissue pathology in farmed Chinook salmon, and that regions of hyper-intense signal indicative of musculoskeletal pathology (Garcia, 2000; May et al., 2000; Steinbach et al., 1994; Theodorou et al., 2012) were significantly associated with both the presence of spinal curvatures and histologically-evident inflammation and fibrosis. These findings support the proposed hypothesis and provide evidence of a direct relationship between spinal curvature and soft-tissue pathology.

MRI ROIs were detected more frequently in individuals with spinal curvature and were strongly associated with curvature location. Since locomotion in salmonids and other finfish is achieved via the closely coupled actions of the spinal column and skeletal musculature (Kisia & Onyango, 2005), these associations may reflect the relative involvement of different spinal regions in swimming. As Chinook salmon and other salmonids exhibit sub-carangiform swimming, the

Journal of Fish Diseases


**TABLE 4** Associations between pathologic magnetic resonance imaging (MRI) region of interest (ROI) types (A–C) and histological lesion types (1–3) in farmed Chinook salmon (*Oncorhynchus tshawytscha*).

| | Histological lesion type | | | | |
|---|---|---|---|---|---|
| MRI ROI type | No histological lesions | 1 | 2 | 3 | Total |
| A | 10 | 24* | 8 | 1 | 43 |
| B | 4 | 1 | 6* | 2 | 13 |
| C | 0 | 0 | 1 | 3 | 4 |
| Total | 14 | 25 | 15 | 6 | 60 |

*Note*: $n = 46$. Asterisks (*) indicate statistically significant associations between MRI ROI type (A, B, C) and histological lesion type (1, 2, 3) as determined by Fisher's exact test with post-hoc Bonferroni correction.

abdominal and posterior spinal regions are heavily recruited, while regions near the head have little involvement. The tail region (R3) in particular is expected to experience the greatest mechanical forces and the post-cranial region (R1) the least (Fjelldal, Hansen, et al., 2009). In the current study, almost half of MRI ROIs were detected in R3, where curvature prevalence was highest, while just two were observed in the post-cranial region (R1), which had the lowest curvature prevalence of the four identified spinal regions. Patterns in the prevalence of spinal curvature and MRI signal hyper-intensity may therefore be reflective of application of different forces in the different regions of spinal column. This has been postulated to explain regional differences in the development of vertebral compression in Atlantic salmon (Fjelldal, Hansen, et al., 2009). A recent study examining the effects of exercise training on the physiology of Chinook salmon also demonstrated differences in swimming dynamics between individuals with and without mild scoliosis (Prescott et al., 2023). Affected individuals were observed to invest greater effort in achieving a given swimming speed, took longer to recover from exhaustive exercise, and had a different muscle fibre and body composition compared to individuals without curvature (Prescott et al., 2023). Observations from both the current and previous studies therefore collectively suggest that swimming mechanics and curvature are linked, but further research is required to understand how forces generated during swimming are related to the development of curvature and the associated soft-tissue pathology.

Three different types of signal hyper-intensity (ROIs) were detected on MRI scans. Histological examination confirmed that these types represented various stages of inflammation and fibrosis. Type A lesions were the most common and presented as a bright unilateral signal which was highly localized to the peri-vertebral connective tissues and associated septa, particularly the horizontal septum. Localized pathologic signal hyper-intensity on T2-weighted MRI scan images is strongly indicative of edema, the accumulation of fluid that occurs as an acute inflammatory response to soft-tissue trauma (Garcia, 2000; Kumar et al., 2016; Steinbach et al., 1994; Theodorou et al., 2012; Winkler et al., 2011). Type A signal was significantly associated with Type 1 histological lesions, which exhibited a high water content and loosely arranged connective tissue indicative of edema and early fibrosis respectively. Munday et al. (2016) observed similar histological lesions: Chinook salmon with spinal curvature exhibited unilateral fibrosis confined to the peri-vertebral connective tissues and horizontal septum. However, few individuals in Munday et al. (2016) were observed to have the accompanying basophilic material, which the authors postulated to be exudate (fluid leakage) indicative of early-stage inflammation. Thus, while the age and size of individuals in the current study are consistent with that of the individuals examined in Munday et al. (2016), they appear to have presented with earlier stages of the inflammatory process. This could be due to variation in the timing of influence of factors that contribute to the inflammation, or possibly genetic differences in susceptibility and/or inflammatory response between the populations. Alternatively, areas containing basophilic material may have been present in more individuals in Munday et al., (2016), but may not have been captured due to the non-targeted sampling approach.

Type B lesions were less prevalent than Type A and were characterized as bilateral, non-localized "cloudy" areas of signal which infiltrated the surrounding skeletal muscle. These signal features were more consistent with mature fibrosis, which is generally considered to follow inflammation and edema as muscular injury resolves, and thus presents as areas of duller MRI signal intensity (Steinbach et al., 1994; Theodorou et al., 2012; Winkler et al., 2011). This was supported by the significant association between Type B and Type 2 histological lesions, which presented as dense, regularly-arranged connective tissue in the absence of basophilic material. Unlike Type A, these lesions infiltrated the skeletal musculature, rather than being localized to the peri-vertebral connective tissues and associated septa, which has been previously observed in severely affected fish (Munday et al., 2016). This is consistent with Type B MRI signals representing a more advanced stage of the reparative process than Type A, as mature fibrosis is considered a 'hallmark' of chronic inflammatory response processes (Munday et al., 2016; Saifuddin et al., 1996).

Although they were not significantly associated with any of the identified histological types, Type C ROIs exhibited features of both Type A and B ROIs. The presence of this type therefore could be considered an intermediate stage of the reparative process. However, it more plausibly represents the early stages of a secondary muscular insult, possibly incurred by imposition of muscle forces on the existing fibrotic (Type B) lesion. Indeed, the junction between healed and normal tissues (i.e., area of fibrosis) following recovery from injury often becomes the weakest part of the unit, and thus susceptible to re-injury. In humans, MRI signal hyper-intensity develops in the presence of existing fibrosis after repeated muscle insult, such as in overuse (Steinbach et al., 1994). Recurrent or chronic muscle insult therefore constitutes a vicious cycle of inflammation and subsequent fibrosis, disuse atrophy and fat infiltration, which increases the stiffness of the affected muscle and predisposes it to further injury (Kumar et al., 2016; May et al., 2000; Theodorou et al., 2012).

In humans with scoliosis, the paravertebral muscle on the concave side of the curvature shortens, stiffens, and atrophies, but lengthens and hypertrophies on the convex side (Kim et al., 2013; Saifuddin et al., 1996). This may explain why Type A signal was consistently on the concave side of scoliotic, but not lordotic or kyphotic, curvatures. In salmon, the range of motion is greater in the lateral plane than the dorso-ventral plane, as this facilitates the generation of force required to achieve forward locomotion. The lateral body movements associated with swimming, especially those associated with anaerobic burst swimming, could therefore forcibly cause the shortened muscle on the concave side of the curvature to lengthen and over-exert, resulting in further damage and triggering a secondary inflammatory process. Such processes would be less likely to occur in the presence of lordosis and kyphosis, as there is limited movement of the salmon spine in the vertical plane. Consequently, the high prevalence of soft-tissue pathology in R3 may not necessarily be due to the presence of curvature in general, but scoliosis specifically, which occurred with the highest frequency in this region. Recent evidence provides support for this theory – Prescott et al. (2023) found that the muscle fibre, protein, and lipid composition of the left and right fillets of Chinook salmon with mild scoliosis was significantly different, and was suggested to be the result of differences in muscle contractile forces exerted during swimming. Further investigation of patterns of curvature in relation to swimming behaviour would therefore presumably be beneficial for understanding the importance of swimming behaviour and mechanical force distribution on curvature development.

Collectively, the paired MRI and histology results appear to indicate a chronology of repair from some sort of muscular insult, which either initiates the development of curvature or arises secondarily. Munday et al. (2016) concluded that fibrosis observed in individuals with curvature was likely associated with a chronic inflammatory process. However, in the absence of a definitive cause of the initial inflammation, excessive musculature or high intensity exercise resulting in muscular strain and subsequent damage to the peri-vertebral muscle and connective tissues was proposed. Observations in the current study are consistent with this theory. Muscle exertion beyond the usual range of tensile forces causes rupture of muscle fibres, usually accompanied by haemorrhage, which subsequently initiates a cascade of acute through chronic phases of inflammation, including edema and infiltration and proliferation of inflammatory and stem cells with fibroblastic potential (Steinbach et al., 1994). The latter forms neo-collagen, which, after cross-linking, matures into "scar tissue" that persists long after the acute inflammatory response has resolved. This process is reflected in the early fibrosis and basophilic material observed in Type A MRI ROIs and the subsequent mature fibrosis that characterized Type B ROIs.

Condition factor has been consistently cited as a risk factor for curvature development in Chinook salmon (Perrott et al., 2020; Scholtens et al., 2023). It is possible that individuals with a high condition factor exert excessive mechanical forces on the spine during swimming, resulting in injury to the spine and the subsequent development of curvature. While there were no observed differences in condition factor between unaffected and affected individuals in the current study, the study population was of harvest-size. Affected individuals therefore likely had possessed curvature for a sustained period, which could have influenced their condition factor (e.g., through malnutrition or body shape distortion). It therefore remains possible that differences in condition factor existed prior to the onset of curvature and could have contributed to its development. Future studies on individuals at earlier stages of production (i.e., immediately prior to the window of radiographic onset of curvature) would help to ascertain this.

Muscle strain generally occurs at the musculo-tendinous junction, which is the weakest part of the muscle-tendon-bone unit due to the reduced elasticity of the muscle at this intersection (Steinbach et al., 1994; Theodorou et al., 2012). In the current study, MRI ROIs and histological lesions were frequently associated with the horizontal and vertical septa, the collagenous sheets of connective tissue primarily responsible for transferring muscular force to the spine (Johnston et al., 2011). This is consistent with the observations of Perrott et al., 2020, who reported that the white (anaerobic) muscle of Chinook salmon from a farmed population with a known high incidence of spinal curvature had a significantly lower Type I collagen content and more immature collagen cross-link profiles – indicative of reduced connective tissue integrity – than individuals from a farm with a low incidence of curvature. Why only Type A signal was associated with the septa remains to be determined, but potentially the initiating inflammatory process develops in the connective tissues and only later affects the surrounding skeletal muscle as fibrotic repair progresses (Munday et al., 2016). High intensity exercise and/or significant muscle growth could theoretically exert excessive muscular force on the connective tissues and/or muscle at the musculo-tendinous junction and compromise their integrity, resulting in subsequent damage to the associated myotomes (Munday et al., 2016). It is also possible that the observed soft-tissue lesions are driven by compromised integrity of the muscle and/or connective tissues (i.e., without excessive muscular force) due to some sort of failure in their structure or development. As previously suggested by Munday et al. (2016), this failure may either pre-dispose individuals to micro-trauma, or occur as a result. While the contributing factors remain to be identified, previous studies of spinal curvature in farmed Chinook salmon have cited genetics, inadequate nutrition, high-intensity exercise, fast growth, sexual maturation, infectious agents, and temperature as being of potential importance (Lovett et al., 2020; Munday et al., 2016). Further research to characterize the development and integrity of muscle and connective tissues in farmed Chinook salmon with and without curvature and understand the influence of such factors on these processes, both prior to and following curvature onset, could therefore help to identify the cause(s) of curvature.

Whether the proposed muscle strain occurs before or after the development of curvature cannot be determined in the current study, given experimental individuals were only examined at one point in time – harvest. At this point, curvatures would have been at an advanced stage of development. However, the results suggest the soft-tissue changes may develop first, as nearly a third of the ROIs (28.33%) were detected in spinal regions without radiographic curvature. Most of these ROIs were Type A and came from the two individuals with MRI ROIs that had no evidence of rSC. These findings are similar to those previously reported by Munday et al. (2016), where peri-vertebral fibrosis was observed in five individuals without radiographic spinal curvature. These individuals may have been at an earlier stage of the inflammatory response – i.e., before the fibrosis or curvature had established. Consequently, there is some evidence to suggest that the inflammatory changes may drive the development of curvature, rather than arising secondarily. It seems plausible that peri-vertebral fibrotic lesions incurred by a chronic inflammatory process could cause an imbalance of muscular forces on the spine and produce curvature. Asymmetric loading of mechanical forces has been previously proposed as a mechanism for spinal curvature development in this species (Perrott et al., 2018), and recent observations by Prescott et al. (2023) support this theory. In the absence of measurement of these forces, we can only speculate on their relative importance to curvature development, but future research could help elucidate this.

Some of the MRI ROIs were histologically normal, but this was likely because many Type A lesions were observed on only 1–2 slices in a given MRI scan ROI, while the histological sample blocks excised from ROIs often measured several centimetres across. Small lesions could therefore have gone undetected. Alternately, some of the regions without pathologic hyper-intense MRI signal were found to have histological lesions, suggesting that these may have been true lesions that simply were not significant enough to produce a signal on MRI.

The observed associations between curvature and inflammatory and fibrotic lesions detected on MRI scans provide evidence that soft-tissue pathology is directly associated with the development of spinal curvature, and may be related to a mechanical loading issue. Further investigation is therefore required to evaluate a possible mechanical aetiology. Torpy et al. (2023) recently demonstrated that both MRI and CT imaging can be used to diagnose musculoskeletal ailments in large live fish – in their case a 13 kg Showa koi (*Cyprinus carpio*) with a spinal injury involving vertebral subluxation and associated spinal cord myelomalacia (softening). While future technological advancements are required to make MRI more accessible and user friendly (i.e., portability), it is nevertheless a valuable tool for the future investigation of finfish musculoskeletal health and conditions, including spinal curvature. For farmed New Zealand Chinook salmon, the progression of soft-tissue changes associated with curvature development can continue to be interrogated using MRI by lethally sampling and scanning a subset of individuals from the same population at frequent intervals throughout seawater production. This targeted sampling and the resulting information may then be used to infer whether the changes occur secondarily or prior to curvature development, and therefore whether further research should focus predominantly on bone (i.e., skeletal) or soft tissues (i.e., neuromuscular) as the primary affected tissue.

## AUTHOR CONTRIBUTIONS

**Bailey A. Lovett:** Conceptualization; investigation; writing – original draft; methodology; visualization; writing – review and editing; formal analysis; project administration; data curation; funding acquisition. **Elwyn C. Firth:** Conceptualization; writing – review and editing; supervision; resources; funding acquisition; investigation. **Matthew R. Perrott:** Methodology; validation; resources; formal analysis; investigation; writing – review and editing. **John S. Munday:** Investigation; methodology; validation; writing – review and editing; formal analysis; resources. **Beau P. Pontre:** Methodology; visualization; software; resources; writing – review and editing; investigation. **Anna-Maria P. Lydon:** Investigation; methodology; visualization; writing – review and editing; software; resources. **Jane E. Symonds:** Funding acquisition; writing – review and editing; supervision; investigation. **Mark A. Preece:** Resources; funding acquisition; writing – review and editing; supervision. **Neill A. Herbert:** Conceptualization; investigation; funding acquisition; writing – review and editing; supervision; resources.

## ACKNOWLEDGEMENTS

This study was funded by the Ministry for Primary Industries [Sustainable Farming Fund (SFF) Project #13/003: Reducing malformations in farmed king salmon], The University of Auckland Institute of Marine Science [Department Seed fund #35023.001] and Callaghan Innovation [R & D Student Research Fellowship #NZKSC1401 to B.A.L.]. We are grateful to Seumas Walker (Cawthron Institute) and Stuart Anderson and Graeme Aldridge of The New Zealand King Salmon Company Ltd. (NZKS) for their generous help in selecting and collecting the experimental animals, and Zac Waddington (NZKS) for his feedback on the manuscript prior to submission. We are also grateful to the University of Auckland Centre of Magnetic Resonance Imaging (CAMRI) for the use of their MRI equipment and their valuable time and expertise, Troy Goodall (Troy Goodall Photography) and Finn Sumner for optimizing the MRI scan images for publication, and Javier Atalah (Cawthron Institute) for his valuable contributions to statistical analysis of the data. We would also like to thank Ian LeGrice and Linley Nisbet (The University of Auckland Department of Physiology) for providing lab space, consumables and support for carcass dissection and decalcification of tissue for histology, and Evelyn Lupton (Massey University) for preparing the tissue sections for histological analysis. Finally, we would like to thank the SFF Salmon Improvement Group (SIG) for their ongoing support throughout the investigation and manuscript preparation. Open access publishing facilitated by The University of Auckland, as part of the Wiley - The University of Auckland agreement via the Council of Australian University Librarians.

## FUNDING INFORMATION

This study was funded by the Ministry for Primary Industries [Sustainable Farming Fund (SFF) Project #13/003: Reducing malformations in farmed king salmon], the University of Auckland Institute of Marine Science [department seed fund #35023.001] and Callaghan Innovation [R & D Student Research Fellowship #NZKSC1401 to B.A.L.].

## CONFLICT OF INTEREST STATEMENT

Bailey Lovett reports equipment, drugs, or supplies and travel were provided by New Zealand King Salmon Co Ltd. Mark Preece reports a relationship with New Zealand King Salmon Co. Ltd. that includes employment.

## DATA AVAILABILITY STATEMENT

The data that support the findings of this study are available from the corresponding author upon reasonable request.

## ORCID

*John S. Munday* https://orcid.org/0000-0002-4769-5247

## REFERENCES

Asperio, R. M., Marzola, P., Zibellini, E., Villa, W., Sbarbati, A., Osculati, F., & Addis, F. (1999). Use of magnetic resonance imaging for diagnosis of a spinal tumor in a cat. *Veterinary Radiology & Ultrasound*, *40*, 267–270.

Bock, C., Sartoris, F.-J., & Pörtner, H.-O. (2002). In vivo MR spectroscopy and MR imaging on non-anaesthetized marine fish: Techniques and first results. *Magnetic Resonance Imaging*, *20*, 165–172.

Bock, C., Sartoris, F. J., Wittig, R.-M., & PoÈrtner, H.-O. (2002). Temperature-dependent pH regulation in stenothermal Antarctic and eurythermal temperate eelpout (Zoarcidae): An in-vivo NMR study. In W. Arntz & A. Clarke (Eds.), *Ecological studies in the Antarctic Sea ice zone* (pp. 266–271). Springer.

Boglione, C., Gisbert, E., Gavaia, P., Witten, E. P., Moren, M., Fontagné, S., & Koumoundouros, G. (2013). Skeletal anomalies in reared European fish larvae and juveniles. Part 2: Main typologies, occurrences and causative factors. *Reviews in Aquaculture*, *5*, S121–S167.

Branson, E. J., & Turnbull, T. (2008). Welfare and deformities in fish. In E. J. Branson (Ed.), *Fish welfare* (pp. 202–216). Blackwell Publishing Ltd.

Collewet, G., Bugeon, J., Idier, J., Quellec, S., Quittet, B., Cambert, M., & Haffray, P. (2013). Rapid quantification of muscle fat content and subcutaneous adipose tissue in fish using MRI. *Food Chemistry*, *138*, 2008–2015.

da Costa, R. C. (2010). Cervical spondylomyelopathy (Wobbler syndrome) in dogs. *Veterinary Clinics: Small Animal Practice*, *40*, 881–913.

Divanach, P., Boglione, C., Menu, B., Koumoundouros, G., Kentouri, M., & Cataudella, S. (1996). Abnormalities in finfish mariculture: An overview of the problem, causes and solutions. In B. Chatain, M. Saroglia, & J. Sweetman (Eds.), *Handbook of Contributions and Short Communications, International Workshop on Sea Bass and Sea Bream Culture: Problems and Prospects* (pp. 45–66). European Aquaculture Society (EAS).

Dyson, S., Murray, R., & Schramme, M. (2005). Lameness associated with foot pain: Results of magnetic resonance imaging in 199 horses (January 2001–December 2003) and response to treatment. *Equine Veterinary Journal*, *37*, 113–121.

Fjelldal, P. G., Hansen, T., Breck, O., Sandvik, R., Waagbø, R., Berg, A., & Ørnsrud, R. (2009). Supplementation of dietary minerals during the early seawater phase increase vertebral strength and reduce the prevalence of vertebral deformities in fast-growing under-yearling Atlantic salmon (*Salmo salar* L.) smolt. *Aquaculture Nutrition*, *15*, 366–378.

Fjelldal, P. G., Hansen, T. J., & Berg, A. E. (2007). A radiological study on the development of vertebral deformities in cultured Atlantic salmon (*Salmo salar* L.). *Aquaculture*, *273*, 721–728.

Fjelldal, P. G., van der Meeren, T., Jørstad, K. E., & Hansen, T. J. (2009). A radiological study on vertebral deformities in cultured and wild Atlantic cod (*Gadus morhua*, L.). *Aquaculture*, *289*, 6–12.

Garcia, J. (2000). MRI in inflammatory myopathies. *Skeletal Radiology*, *29*, 425–438.

Gnirs, K., Ruel, Y., Blot, S., Begon, D., Rault, D., Delisle, F., Boulouha, L., Colle, M. A., Carozzo, C., & Moissonnier, P. (2003). Spinal sub arachnoid cysts in 13 dogs. *Veterinary Radiology & Ultrasound*, *44*, 402–408.

Gonçalves, R., Platt, S. R., Llabrés-Díaz, F. J., Rogers, K. H., de Stefani, A., Matiasek, L. A., & Adams, V. J. (2009). Clinical and magnetic resonance imaging findings in 92 cats with clinical signs of spinal cord disease. *Journal of Feline Medicine and Surgery*, *11*, 53–59.

Grünenfelder, F. I., Weishaupt, D., Green, R., & Steffen, F. (2005). Magnetic resonance imaging findings in spinal cord infarction in three small breed dogs. *Veterinary Radiology & Ultrasound*, *46*, 91–96.

Hansen, T., Fjelldal, P., Yurtseva, A., & Berg, A. (2010). A possible relation between growth and number of deformed vertebrae in Atlantic salmon (*Salmo salar* L.). *Journal of Applied Ichthyology*, *26*, 355–359.

Howell, N., Shavila, Y., Grootveld, M., & Williams, S. (1996). High-resolution NMR and magnetic resonance imaging (MRI) studies on fresh and frozen cod (*Gadus morhua*) and haddock (*Melanogrammus aeglefinus*). *Journal of the Science of Food and Agriculture*, *72*, 49–56.

Huntingford, F. A., Adams, C., Braithwaite, V., Kadri, S., Pottinger, T., Sandøe, P., & Turnbull, J. (2006). Current issues in fish welfare. *Journal of Fish Biology*, *68*, 332–372.

Johnston, I., Bower, N., & Macqueen, D. (2011). Growth and the regulation of myotomal muscle mass in teleost fish. *Journal of Experimental Biology*, *214*, 1617–1628.

Joseph, S. Y., & Habib, P. (2009). MR imaging of urgent inflammatory and infectious conditions affecting the soft tissues of the musculoskeletal system. *Emergency Radiology*, *16*, 267–276.

Kattapuram, T. M., Suri, R., Rosol, M. S., Rosenberg, A. E., & Kattapuram, S. V. (2005). Idiopathic and diabetic skeletal muscle necrosis: Evaluation by magnetic resonance imaging. *Skeletal Radiology*, *34*, 203–209.

Keeble, E. (2006). Common neurological and musculoskeletal problems in rabbits. *In Practice*, *28*, 212–218.

Kim, H., Lee, C.-K., Yeom, J. S., Lee, J. H., Cho, J. H., Shin, S. I., Lee, H.-J., & Chang, B.-S. (2013). Asymmetry of the cross-sectional area of paravertebral and psoas muscle in patients with degenerative scoliosis. *European Spine Journal*, *22*, 1332–1338.

Kisia, S. M., & Onyango, D. W. (2005). *Muscular system of vertebrates* (p. 115). Science Publishers Inc.

Koumoundouros, G. (2010). Morpho-anatomical abnormalities in Mediterranean marine aquaculture. *Recent Advances in Aquaculture Research*, *66*, 125–148.

Kumar, Y., Wadhwa, V., Phillips, L., Pezeshk, P., & Chhabra, A. (2016). MR imaging of skeletal muscle signal alterations: Systematic approach to evaluation. *European Journal of Radiology*, *85*, 922–935.

Lannig, G., Bock, C., Sartoris, F. J., & Portner, H. O. (2004). Oxygen limitation of thermal tolerance in cod, *Gadus morhua* L., studied by magnetic resonance imaging and on-line venous oxygen monitoring. *American Journal of Physiology. Regulatory, Integrative and Comparative Physiology*, *287*, R902–R910.

Lovett, B. A., Firth, E. C., Plank, L. D., Symonds, J. E., Preece, M. A., & Herbert, N. A. (2019). Investigating a relationship between body composition and spinal curvature in farmed adult New Zealand king salmon (*Oncorhynchus tshawytscha*): A novel application of dual-energy X-ray absorptiometry. *Aquaculture*, *502*, 48–55.

Lovett, B. A., Firth, E. C., Tuck, I. D., Symonds, J. E., Walker, S. P., Perrott, M. R., Davie, P. S., Munday, J. S., Preece, M. A., & Herbert, N. A.

(2020). Radiographic characterisation of spinal curvature development in farmed New Zealand Chinook salmon Oncorhynchus tshawytscha throughout seawater production. *Scientific Reports*, *10*(1), 20039.

Lu, D., Lamb, C., Wesselingh, K., & Targett, M. (2002). Acute intervertebral disc extrusion in a cat: Clinical and MRI findings. *Journal of Feline Medicine and Surgery*, *4*, 65–68.

MacKay, A. D., Rusbridge, C., Sparkes, A. H., & Platt, S. R. (2005). MRI characteristics of suspected acute spinal cord infarction in two cats, and a review of the literature. *Journal of Feline Medicine and Surgery*, *7*, 101–107.

Mahoney, P. (2012). Musculoskeletal imaging in the cat: What's normal? What's abnormal? *Journal of Feline Medicine and Surgery*, *14*, 13–22.

Mark, F. C., Bock, C., & Portner, H. O. (2002). Oxygen-limited thermal tolerance in Antarctic fish investigated by MRI and 31P-MRS. *American Journal of Physiology. Regulatory, Integrative and Comparative Physiology*, *283*, R1254–R1262.

May, D. A., Disler, D. G., Jones, E. A., Balkissoon, A. A., & Manaster, B. (2000). Abnormal signal intensity in skeletal muscle at MR imaging: Patterns, pearls, and pitfalls. *Radiographics*, *20*, S295–S315.

Mitchell, C. W., Nykamp, S. G., Foster, R., Cruz, R., & Montieth, G. (2012). The use of magnetic resonance imaging in evaluating horses with spinal ataxia. *Veterinary Radiology & Ultrasound*, *53*, 613–620.

Munday, J. S., Perrott, M. R., Symonds, J. E., Walker, S. P., Lovett, B., Preece, M. A., & Davie, P. S. (2016). Unilateral perivertebral fibrosis associated with lordosis, kyphosis and scoliosis (LKS) in farmed Chinook salmon in New Zealand. *Diseases of Aquatic Organisms*, *121*, 211–221.

Murphy, W. A., Totty, W., & Carroll, J. E. (1986). MRI of normal and pathologic skeletal muscle. *American Journal of Roentgenology*, *146*, 565–574.

Perrott, M., Lovett, B. A., De Clercq, A., Davie, P. S., Munday, J. S., Morel, P. C. H., Preece, M. A., Symonds, J. E., Walker, S. P., Loo, T., & Norris, G. (2020). Type I collagen differences in farmed Chinook salmon (*Oncorhynchus tshawytscha*) in New Zealand. *Aquaculture*, *525*, 735264.

Perrott, M., Symonds, J., Walker, S., Hely, F., Wybourne, B., Preece, M., & Davie, P. (2018). Spinal curvatures and onset of vertebral deformities in farmed Chinook salmon, *Oncorhynchus tshawytscha* (Walbaum, 1792) in New Zealand. *Journal of Applied Ichthyology*, *34*, 501–511.

Pörtner, H.-O., Mark, F. C., & Bock, C. (2004). Oxygen limited thermal tolerance in fish? Answers obtained by nuclear magnetic resonance techniques. *Respiratory Physiology & Neurobiology*, *141*, 243–260.

Prescott, L. A., Symonds, J. E., Walker, S. P., Miller, M. R., Semmens, J. M., & Carter, C. G. (2023). Long-term sustained swimming improves swimming performance in Chinook salmon, *Oncorhynchus tshawytscha*, with and without spinal scoliosis. *Aquaculture*, *574*, 739629.

Rogers, B. L., Lowe, C. G., Fernandez-Juricic, E., & Frank, L. R. (2008). Utilizing magnetic resonance imaging (MRI) to assess the effects of angling-induced barotrauma on rockfish (Sebastes). *Canadian Journal of Fisheries and Aquatic Sciences*, *65*, 1245–1249.

Saifuddin, A., Sherazi, Z., Shaikh, M., Natali, C., Ransford, A., & Pringle, J. (1996). Spinal osteoblastoma: Relationship between paravertebral muscle abnormalities and scoliosis. *Skeletal Radiology*, *25*, 531–535.

Scholtens, M., Dodds, K., Walker, S., Clarke, S., Tate, M., Slattery, T., Preece, M., Arratia, L., & Symonds, J. (2023). Opportunities for improving feed efficiency and spinal health in New Zealand farmed Chinook salmon (*Oncorhynchus tshawytscha*) using genomic information. *Aquaculture*, *563*, 738936.

Silverstone, A. M., & Hammell, L. (2002). Spinal deformities in farmed Atlantic salmon. *The Canadian Veterinary Journal*, *43*, 782–784.

Simões, J. M., Teles, M. C., Oliveira, R. F., Van der Linden, A., & Verhoye, M. (2012). A three-dimensional stereotaxic MRI brain atlas of the cichlid fish *Oreochromis mossambicus*. *PLoS One*, *7*, e44086.

Steinbach, L. S., Fleckenstein, J. L., & Mink, J. H. (1994). Magnetic resonance imaging of muscle injuries. *Orthopedics*, *17*, 991–999.

Sullivan, M., Hammond, G., Roberts, R., & Manchester, N. (2007). Spinal deformation in commercially cultured Atlantic salmon, *Salmo salar* L.: A clinical and radiological study. *Journal of Fish Diseases*, *30*, 745–752.

Theodorou, D., Theodorou, S., & Kakitsubata, Y. (2012). Skeletal muscle disease: Patterns of MRI appearances. *The British Journal of Radiology*, *85*, e1298–e1308.

Torpy, F. J., Comolli, J. R., Gendron, K. P., Armwood, A. R., Camus, A. C., Kehoe, S. R., & Divers, S. J. (2023). Use of computed tomography and magnetic resonance imaging to assess a case of spinal injury in a Showa koi *Cyprinus carpio*. *Journal of Aquatic Animal Health*, *35*(1), 11–19.

Tucker, R. L., & Sande, R. D. (2001). Computed tomography and magnetic resonance imaging in equine musculoskeletal conditions. *Veterinary Clinics of North America: Equine Practice*, *17*, 145–157.

Vagsholm, I., & Djupvik, H. (1998). Risk factors for spinal deformities in Atlantic salmon, *Salmo salar* L. *Journal of Fish Diseases*, *21*, 47–53.

Van der Linden, A., Verhoye, M., Pörtner, H.-O., & Bock, C. (2004). The strengths of in vivo magnetic resonance imaging (MRI) to study environmental adaptational physiology in fish. *Magnetic Resonance Materials in Physics, Biology and Medicine*, *17*, 236–248.

Waagbø, R., Kryvi, H., Breck, O., & Ørnsrud, R. (2005). *Final Report NFR#164773. Bone disorders in intensive aquaculture of Salmon and Cod Workshop* (p. 42). NIFES.

Wei, F., Zhong, R., Zhou, Z., Wang, L., Pan, X., Cui, S., Zou, X., Gao, M., Sun, H., & Chen, W. (2014). In vivo experimental intervertebral disc degeneration induced by bleomycin in the rhesus monkey. *BMC Musculoskeletal Disorders*, *15*, 340.

Winkler, T., von Roth, P., Matziolis, G., Schumann, M. R., Hahn, S., Strube, P., Stoltenburg-Didinger, G., Perka, C., Duda, G. N., & Tohtz, S. V. (2011). Time course of skeletal muscle regeneration after severe trauma: Muscle function against the background of MRI and histological findings. *Acta Orthopaedica*, *82*, 102–111.

Witten, P. E., Gil-Martens, L., Huysseune, A., Takle, H., & Hjelde, K. (2009). Towards a classification and an understanding of developmental relationships of vertebral body malformations in Atlantic salmon (*Salmo salar* L.). *Aquaculture*, *295*, 6–14.

Wu, J.-L., Zhang, J.-L., Du, X.-X., Shen, Y.-J., Lao, X., Zhang, M.-L., Chen, L.-Q., & Du, Z.-Y. (2015). Evaluation of the distribution of adipose tissues in fish using magnetic resonance imaging (MRI). *Aquaculture*, *448*, 112–122.

Zubrod, C. J., Schneider, R. K., Tucker, R. L., Gavin, P. R., Ragle, C. A., & Farnsworth, K. D. (2004). Use of magnetic resonance imaging for identifying subchondral bone damage in horses: 11 cases (1999–2003). *Journal of the American Veterinary Medical Association*, *224*, 411–418.

**How to cite this article:** Lovett, B. A., Firth, E. C., Perrott, M. R., Munday, J. S., Pontre, B. P., Lydon, A.-M., Symonds, J. E., Preece, M. A., & Herbert, N. A. (2024). Magnetic resonance imaging shows spinal curvature in Chinook salmon (*Oncorhynchus tshawytscha*) is associated with chronic inflammation of peri-vertebral soft tissues. *Journal of Fish Diseases*, *47*, e13900. https://doi.org/10.1111/jfd.13900